LIMNOLOGY
and
OCEANOGRAPHY

ASLO

Limnol. Oceanogr. 00, 2015, 00–00

doi: 10.1002/lno.10086

Modeling circulation and seasonal fluctuations in perennially ice-covered and ice-walled Lake Untersee, Antarctica

H. C. B. Steel,[1] C. P. McKay,[1] D. T. Andersen*[2]
[1]MS-245-3 NASA Ames Research Center Moffett Field, California
[2]Carl Sagan Center, SETI Institute, Mountain View, California

Lake Untersee, Antarctica, is a freshwater perennially ice covered lake bounded along its north by the Anuchin glacier. The Massachusetts Institute of Technology general circulation model, used on a representative wedge-shaped lake and actual bathymetry for Lake Untersee, produces estimates for circulation and long-term temperature and mixing trends. Modeled circulation is dominated by an anticyclonic gyre in front of the glacier, with slower $\sim$ 3 mm s^{-1} flow exhibited around the lake's perimeter, allowing effective mixing throughout most of the lake with time scales of one month. Estimated velocities bound maximal glacial flour particle size at $\sim$ 10 μm for effective transport throughout the lake, consistent with the sediment's mostly fine composition observed in field studies, and mixing time scales mean nonuniformities in measured O_2 concentration likely require recent or ongoing sources. Areas in which large temperature gradients prevent exchange of fluid demonstrate minimal mixing, such as the lake's upper water layers and the anoxic basin in the south, and circulation is consistently slowed in the northern sheltered bay area. Mean flow velocities fluctuate by about one fifth of their magnitude between summer and winter, and the lake's almost homothermal body temperature varies by about one tenth of a degree over the same period. While calculated temperature profiles qualitatively agree with field data, the model's long-term equilibrium temperature differs substantially, likely due to poor description of heat transfer with the glacier. Model robustness tests show results differ by $\sim$ 10% when either grid scale or water temperature are halved.

Lake Untersee in East Antarctica is a perennially ice covered, ultra-oligotrophic lake partially walled by glacier ice, and has attracted study owing to, among other factors, the presence of large conical stromatolites on its floor, the high pH of its water column, and the presence of extremely high levels of dissolved methane in the anoxic bottom waters (Wand et al. 2006; Andersen et al. 2011). Due to a remote location and challenging environment, little is known about many aspects of the lake, in particular its circulation dynamics and thermal structure, factors that have a major impact on the horizontal and vertical movement of fine-grained sediments, nutrients, and dissolved gases and hence ecosystem function and ultimately lacustrine productivity. Furthermore, ice-covered lakes generally present flow speeds of magnitude $\sim 10^{-3}$ m s^{-1} (Kirillin et al. 2012), which due to the resolution and accuracy of field equipment suitable for such environments, may be difficult to measure. Lakes, including perennially ice-covered lakes exhibit spatial heterogeneity at a variety of temporal and spatial scales, and changes in the physical structure of the water column as a result of the controls exerted by ice-walls and ice-covers will ultimately shape the biological communities and ecosystem processes (Simmons et al. 1993; MacIntyre and Melack 1995; Kratz et al. 2005).

In the context of this discussion we can consider four categories of lakes: open-water lakes, seasonally ice-covered lakes, perennially ice-covered lakes, and perennially ice-covered lakes in contact with a wall of ice. Open water lakes have circulation that is predominantly wind-driven, resulting in significantly larger velocities and mixing rates. Seasonally ice-covered lakes are wind driven during their open-water season, and circulation is driven by thermal gradients once a substantial ice-cover is in place as they are shielded from wind (Huttula et al. 2010). In addition, large water temperature fluctuations are exhibited throughout the year, allowing substantial sediment heat fluxes during ice-covered periods (Fang and Stefan 1996), which are found to be significant drivers of circulation (Kirillin et al. 2012; Rizk et al. 2014). Perennially ice-covered lakes are protected from wind and temperature changes as large as those in seasonally ice-covered lakes by their ice-cover, and are often stratified, from a 0°C boundary condition at the surface, to bottom temperatures of $\sim$4°C, corresponding to the maximum density point of water. Perennially ice-covered ice-walled lakes

*Correspondence: dandersen@seti.org

are in some regards similar to perennially ice-covered lakes, the ice surface shields them from wind and large temperature fluctuations, however the presence of an ice wall introduces an additional boundary condition, which prevents a static thermal stratification. Water at 4°C, which would usually sink and remain at the lake's bottom, is cooled and driven upward by the ice wall, resulting in a constant overturning. This keeps ice-covered lakes well mixed, as is observed in Lake Untersee (Wand et al. 2006) and means their dynamics differ markedly from the other three broad categories of lakes.

Approximated as a box bounded on one side by an ice wall, such lakes draw parallels with the work of Küblbeck et al. (1980) involving numerical simulation of free convection in cavities, and experiments studying convection in a small box due to side-heating by Belmonte et al. (1995). Hossain and Rees (2005) considered similar problems for water near its density maximum, while Yoon et al. (2009) studied thermosolutal convection in a square cavity with salting from above. Wilson and Lee (1981) considered flow driven by an ice wall, finding upward motion for body water temperatures below the maximum density point of water.

Farmer and Carmack (1981) demonstrated the effects of temperatures near the maximum density point of water mixing in an open water lake, finding pressure effects play an important role in dynamics near this point due to a decreased coefficient of expansion. Patterson and Hamblin (1988) added ice and snow cover to an existing lake mixing model, demonstrating the importance of coupling between ice cover and underlying water, and comparing this with data from Lake Laberge and Babine Lake in Canada.

Malm et al. (1998) and Petrov et al. (2007) performed field studies on seasonally ice covered Lake Vendyurskoe, Russia, finding currents generally on the order of millimetres per second but ranging up to $\sim$ 1 cm s^{-1}. They were hypothesized as being, due to lack of inflows into the lake, a result of horizontal temperature (pressure) gradients, and were found to be geostrophic in nature. Rizk et al. (2014) combined field observations with theoretical analysis of Lake Pääjärvi, Finland, again finding velocities $\sim 10^{-3}$m s^{-1}, and observing geostrophic circulation in the form of basin-scale anti-cyclonic or cyclonic gyres. Huttula et al. (2010) used the Princeton Ocean Model to study the same lake, as well as a simplified conical basin, finding good agreement between modeled and observed results, estimating mean flow velocities of 0.85 cm s^{-2}, and anticipating circulation in upper water layers as being anticyclonic, and that of deep layers cyclonic. While most studies have concentrated on Arctic lakes due to their relative abundance and ease of access, Tyler et al. (1998) studied perennially ice-covered Lakes Hoare and Fryxell in the McMurdo Dry Valley region of Antarctica, providing evidence in the form of chlorofluorocarbon concentration profiles for mixing throughout the water column, with vertical mixing time scales of 20-30 yr, and Wüest and Carmack (2000) made theoretical estimates of mixing and circulation in Lake Vostok, estimating both horizontal and vertical velocity scales of $\sim$ 0.3 mm s^{-1}.

In this study, we use the Massachusetts Institute of Technology general circulation model (Marshall et al. 1997; referred to from here as MITgcm), along with packages developed by others, to compute the circulation for two lakes. First, we consider an idealized wedge shaped ice-walled and ice-covered lake (henceforth referred to as the idealized simulation), and second, we consider both higher- (referred to as Untersee–hires) and lower- (referred to as Untersee–lowres) resolution models of Lake Untersee including the perennial ice cover, the glacial wall bounding the lake, and actual bathymetry. The MITgcm has been used in open ocean problems on similar scales, such as subaqueous melting of Greenland tidewater glaciers, by Xu et al. (2012), and by Heimbach and Losch (2012) on sub-ice-shelf melt rates and ocean circulation in West Antarctica. It has also found applications in the study of lakes, with model verification and analysis of sensitivity on physical parameters performed by Dorostkar et al. (2010) on Cayuga Lake, New York.

The MITgcm results are combined with theoretical treatment of different facets of the problem, and both are compared with measured properties of the lake and its environment to assess their accuracy. The impact of a substantially sized ice wall on long-term mixing and temperature dynamics is considered, the results of which may provide insight into the behavior of (and effect on life in) similar lakes elsewhere in the Antarctic, the Arctic, and in glacial damned fjords. In addition, our solution for circulation in an enclosed waterbody with an isothermal wall may be translatable to other problems in lake dynamics.

Methods

Location and environmental properties

Lake Untersee (Fig. 1) is located at 71°20′S 13°45′E; 563 m above sea level, in central Dronning Maud Land, Antarctica. It has a surface area of 11.4 km^2 (Andersen et al. 2011), making it one of the largest surface lakes in East Antarctica. The lake consists of two sub-basins (Fig. 1), the north and largest basin which lies adjacent to the face of the Anuchin Glacier, is 169-m deep and is separated from a second basin (to the south), 100-m deep, by a sill at 50-m depth (Wand et al. 1996). The lake is well mixed and oxygenated to the bottom, with the exception of the south basin, in which the water is characterized by a sharp change in pH, temperature and oxygenation, and will hence be referred to as the anoxic basin (Wand et al. 2006). Untersee is perennially ice-covered, with ice thickness ranging from 2.2-3.8 m, averaging 3.0 m in summer, (Wand et al. 1996) and the lake's perennial ice-cover is believed to have existed for more than hundreds of years (Wand and Perlt 1999). The lake is fed primarily by subaquatic inflow from the Anuchin Glacier, and water is

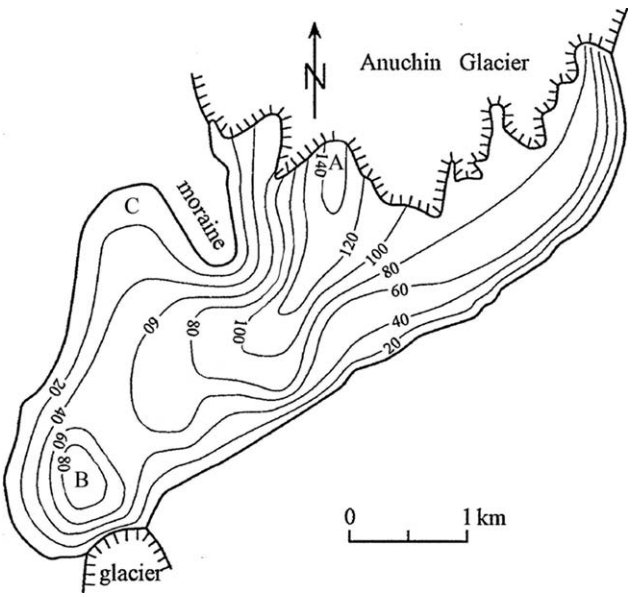

Fig. 1. Lake Untersee Bathymetry for Lake Untersee adapted from Wand et al. (2006). A = North basin/glacier, B = Anoxic basin, C = Sheltered bay area.

lost only by sublimation at the ice surface of the lake (Hermichen et al. 1985). The glacier advances at approximately 9 m per year (Wand et al. 1999), from bathymetry data of Loopmann et al. (1988) we estimate the glacier has a cross sectional area of approximately ~ 0.23 km^2 just prior to entering the lake, and (assuming a vertical ice face following the bottom bathymetry) a subaqueous exposed ice face of ~ 0.68 km^2. The PAR transimissivity for Lake Untersee has been measured at 4.9% (Andersen et al. 2011), and annual average solar radiation at the site is 99 W m^{-2} (Andersen et al. unpubl). Using the description of light attenuation in ice cover proposed by McKay et al. (1994) and the transmission properties of ice over a wider spectral range (Warren and Brandt 2008) the average transmissivity of the ice cover over the solar spectrum at sea level (ASTM Standard G-173 2012) is calculated as 2.6%. Multiplying by the annual solar flux arriving at the ice surface, this gives an annual average of 2.6 W m^{-2} of solar radiation entering the water column, with a daily average of zero during winter, and varying approximately sinusoidally during summer months (Andersen et al. unpubl).

Conductivity, pH, and temperature of lake water were measured in situ using a freshly calibrated Hydrolab DS5 multi-parameter water quality sonde (OTT Hydromet, 5600 Lindbergh Dr., Loveland, CO 80539) lowered through the water column via a 25-cm diameter holes drilled through the ice cover. Measurements were collected at 1-m depth intervals, allowing the sonde to equilibrate before data were recorded at the surface with a portable field computer. Photosynthetically active radiation (PAR) was measured using a LI-Cor LI-192 underwater quantum sensor connected to a LiCor LI-1400 meter (Li-Cor, Lincoln, NB). Readings were taken at 1-m depth intervals as the sensor was lowered although the water column in the deepest part of the two basins. A LI-Cor LI-190 terrestrial quantum sensor was used to obtain simultaneous measures of incident irradiance to allow underwater readings to be recalculated as percentage of surface irradiance. Climate data, including air temperature and humidity above the surface and in soil, wind speed/direction, and incoming and outgoing solar flux were collected using a Campbell meterological station that had been established on the shore of Lake Untersee in 2008 (Andersen et al. unpubl).

Theoretical framework

Mean circulation and velocity

Gill (1982) outlined the requirement that in order for Coriolis acceleration to have substantial impact on circulation, a lake's largest dimension must exceed its Rossby radius of deformation:

$$R_{\mathrm{Ros}} = c/f \tag{1}$$

Here, f= Coriolis frequency, and c= wave speed defined for stable stratification and given by

$$c \approx \frac{ND}{n\pi} \tag{2}$$

where D= water depth, n= number of baroclinic mode, N = Brunt-Väisälä frequency (Gill 1982) given by

$$N^2 = -\frac{g}{\rho_0}\frac{\partial \rho}{\partial z} \tag{3}$$

Using a quadratic equation of state (Farmer and Carmack 1981) and estimates of temperature change with depth in the well-mixed region of Untersee based on measurements by Wand et al. (2006), we find a maximal Rossby Radius ~ 3 km. As this is on the order of the lake's maximal dimension, Coriolis acceleration likely plays an important role in baroclinic motion, as was found by Huttula et al. (2010) in Lake Pääjärvi, where the latitude 61°04′N gives a Coriolis frequency 92% of that at Untersee, and Kirillin et al. (2012) in general for ice lakes with dimensions exceeding 1 km. Furthermore, the Rossby number for circulation, a dimensionless characterization of flow defined as the ratio of inertial to Coriolis forces, is $\sim 10^{-2}$ for length and velocity scales of 1000 m and 1 mm s^{-1}, respectively, again demonstrating domination of geostrophic flow.

Buoyancy driven flow due to a melting ice wall results in a free convection system with upward fluid motion nearest the wall for water with body temperatures less than the maximum density point of water (Fig. 2; Wilson and Lee 1981; Wang and Wang 1988). Wilson et al. (1981), and in more depth, Lee (1979), simulated such systems, finding over

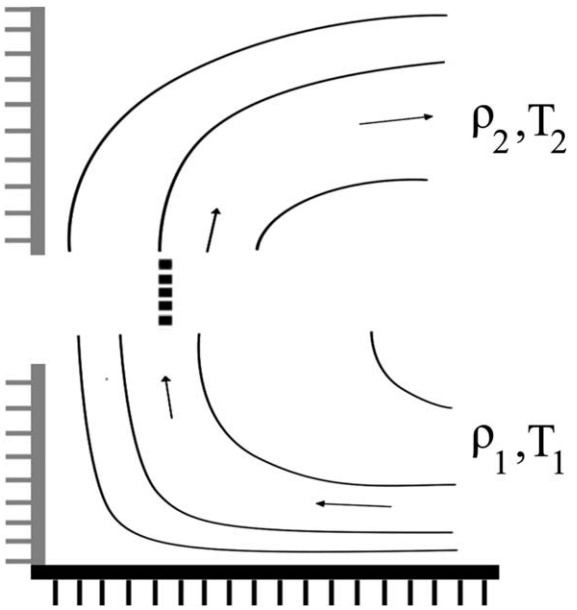

Fig. 2. Streamlines for buoyancy driven flow Water below the 4°C maximum density point is drawn into the ice wall at the base of the system, decreases in density as it cools, and flows upward due to the resulting buoyant force. At or before it reaches the ice cover flow enters surrounding water of a lower temperature $(T_2 < T_1)$ and density $(\rho_2 < \rho_1)$, flow is retarded, and the fluid moves away from the ice wall.

small scales and body temperatures of $\sim$ 0.5 C, as measured in Untersee (Wand et al. 2006), upward velocities of $\sim$ 3 mm s^{-1}, boundary layers of thickness $\sim 10^{-1}$ m and ice wall melting rate $\sim 8\times10^{-8}$m s^{-1}. Also observed is the tendency for a peak in melting rate at the base of flow, where warm water is being drawn into the wall, with a large component of its velocity perpendicular to the ice face. While a good first estimate, this simplistic treatment does not address many factors of the motion (Carey and Gebhat 1980), and in particular does not capture the size and geometry of possible flows in Lake Untersee. Also to be considered is the near-linear dependence of freezing point of water on pressure (Millero 1978), which, at 160-m depth accounts for a decreased freezing point of -0.12°C, potentially significant in calculation of melting rate when compared to Untersee's body temperature.

For velocities of $v \sim$ 2 to 3 mm s^{-1} as estimated above, similar to those found in some ice covered lakes (Malm et al. 1998; Rizk et al. 2014), an average depth $D \sim$ 60 m and a typical kinematic viscosity for pure water at ~ 1°C of $v \sim 1.7\times10^{-6}$m^{2}s^{-1}, the Reynolds number, $Re=vD/v$ is $\sim 5\times10^4$, implying the flow will contain small scale turbulence.

To estimate velocity profiles driven by overflow in the anoxic basin, we use the Blasius solution to laminar boundary layer thickness required for a 99% free stream velocity reduction (Blasius 1908),

$$\delta = 5\times L\times Re^{-0.5} \tag{4}$$

where δ = boundary layer thickness (m), L = length of flow (m), and Re = Reynolds number.

Using temperature profiles measured in Lake Untersee (*see* Fig. 7, Wand et al. 2006) we estimate $\sim$ 50 m depth as the transition into the stagnant region for this calculation, at which point the roughly circular basin has radius $\sim$ 300 m (Estimated form Fig. 1), which is chosen as the value for L, length of flow. Using a velocity of 1.4 mm s^{-1} (*see* Results) and a typical kinematic viscosity at $\sim$4°C for water of $v = 1.55\times10^{-6}$m^{2}s^{-1}, $Re \approx 2.7\times10^5$, demonstrating flow is reaching the verge of turbulence, and giving boundary layer thickness $\delta \approx 3$ m.

Mechanisms of mixing due to overflow at a boundary between fluids can be characterized by the Richardson number:

$$Ri = \frac{\Delta b D}{V^2} \tag{5}$$

Here, V = overflow velocity (m s^{-1}), D = overflow thickness (m), and Δb = buoyancy jump across the interface (m s^{-2}) given by,

$$\Delta b = -g\frac{\Delta\rho}{\rho} \tag{6}$$

where g = acceleration due to gravity ($m\ s^{-1}$), $\Delta\rho$ = density difference across the mixing interface (kg m^{-3}), and ρ_0 = reference density (kg m^{-3}). For $Ri < 1$ buoyancy effects become insignificant and eddy engulfment dominates entrainment, while for $Ri > 20$ buoyancy effects are so strong that entrainment is only due to molecular diffusion (Kirkpatrick et al. 2012). Only for intermediate values will mixing be determined by a buoyancy regulated turbulent boundary layer. Assuming a uniform overflow velocity (V), overflow thickness (D) $\sim$ 50 m (the depth of water above the anoxic basin), and a density difference corresponding to freshwater temperatures 0.5°C and 3.8°C above and below the interface, overflow velocities of 1.4 and 50 mm s^{-1} give $Ri \sim 25,000$ and 20, respectively.

Heat transfer

Jenkins et al. (2001) described the exchange of salt and heat at an ice-ocean interface, taking into account the fact that the ice does not present only a material surface but also an active boundary layer. The rate of freezing or melting is primarily determined by the transfer of heat across this boundary layer, which itself is governed by heat gradient perpendicular to the surface and levels of turbulence, a function of flow rate (Holland and Jenkins 1999). The heat conservation equation for this process, which we assume remains a good approximation in for freshwater if the salinity terms are omitted, is

$$C_{pW}\rho_W\gamma_T|\nu|(T-T_B)=-q\left[L_f+C_{pI}(T_{ice}-T_B)\right] \quad (7)$$

where C_{pW}= heat capacity of water (J $K^{-1}kg^{-1}$), ρ_W = density of water (kg m^{-3}), $|\nu|$ = magnitude of velocity parallel to ice (m s^{-1}), T = waterbody temperature (K), T_B = boundary layer temperature (K), q = melting rate of ice (kg $s^{-1}m^{-2}$), L_f = water latent heat of fusion (J kg^{-1}), C_{pI} = heat capacity of ice (J $K^{-1}kg^{-1}$) and T_{ice} is the ice temperature (K). γ_T is the dimensionless turbulent exchange coefficient, a scaling factor for the effect of velocity on heat transfer, defined as by Holland et al. (2008).

In seasonally ice covered lakes sediments provide thermal inertia by receiving heat during summer then releasing it to the water in winter. This winter return flux can be a substantial driver of dynamics in many cases (Malm et al. 1998; Kirillin et al. 2012). Fang et al. 1996 quantified the effects of this heat exchange (and daily fluctuations) on water temperatures and found it to be noticeable for many lake geometries, with the effect being greater for lakes that are shallower relative to their depth than Lake Untersee. Heat exchange from sediments can be estimated from (Hondzo and Stefan 1994)

$$q=\rho c_p\frac{\partial}{\partial t}\int_0^{z_0}T(z,t)dz \quad (8)$$

where q = heat flux $\left(\text{W m}^{-2}\right)$, ρ = density of sediment kg m^{-3}, c_p = specific heat capacity of sediment J $kg^{-1}K^{-1}$, with $\rho c_p \sim 2.2\times10^6$ J $m^{-3}K^{-1}$ as estimated by Rowland et al. (2011) for lake sediments in permafrost regions, and z_0 = adiabatic boundary depth $\sim$ 10 m for lake sediments (Fang et al. 1996). $T(z,t)$ is the temperature profile of the sediments (°C), found by solving the one dimensional heat equation (Fang et al. 1996) while assuming temperature continuity across the sediment-water interface and that this boundary temperature varies sinusoidally throughout the year (approximating Fig. 4).

$$T(z,t)=T_0+\Delta T_0\exp\left(-z\sqrt{\frac{\omega}{2\kappa}}\right)\sin\left(\omega t-z\sqrt{\frac{\omega}{2\kappa}}\right) \quad (9)$$

where $T_0 \approx 0.72$°C, annual mean bottom temperature (*see* Results, Fig. 4), $\Delta T_0 \approx 0.065$°C , amplitude of annual fluctuations about mean temperature, z = depth in sediment (m), t = time in seconds, ω= frequency of temperature fluctuations (s), equal to 2π divided by year length in seconds, κ= thermal diffusivity of sediments (m^2s^{-1}), equal to the thermal conductivity of sediments divided by the product of their density and specific heat capacity, and estimated for sediments as 1.09×10^{-6} m^2s^{-1} (Rowland et al. 2011).

Combining Eqs. 8 and 9, there is no dependence of q on T_0, the lake's long-term average temperature (due to the time derivative), and Eq. 8 yields six month average sediment heat fluxes from the sediment for summer/winter of $\sim \pm 0.044$ W m^{-2}. Using an average depth of 60 m, incoming annually averaged solar flux of 2.6 W m^{-2} and a water attenuation length of 30 m (Andersen et al. 2011), 14% of the solar radiation (an annual averaged flux of 0.35 W m^{-2}) reaches the lake floor, corresponding to six month averages of twice this amount, 0.7 W m^{-2} in summer, and zero through winter. Therefore, on comparison with the sediment heat fluxes, only $\sim$ 6% of the radiation arriving to the top layer of the sediments is conducted into the ground to drive its seasonal temperature changes, while $\sim$ 94% of the energy is returned to the water. As sediment heat fluxes are of such small magnitude, combined with the fact that they seasonally average to zero, we believe effects of sediment heat transfer will be minor compared to other factors driving the lake's circulation and we neglect it in modeling. It is also assumed that net heat flows away from the sediments, such as those required to sustain a Talik (unfrozen ground beneath a lake in permafrost regions, modeled by Rowland et al. 2011), are minor.

MITgcm modeling

The MITgcm (Marshall et al. 1997), is a scalable finite-volume numerical ocean or lake model, which in this study is used in nonhydrostatic, vertical geopotential (z) height levels, and Cartesian grid configuration. It solves the incompressible Navier–Stokes equations with the Boussinesq approximation, and includes nonlinear equations of state, vertical sub-grid-scale mixing by constant eddy diffusivity or K profile parameterization (KPP) scheme, and horizontal mixing defined by constant eddy viscosities or nonlinear Smagorinsky viscosities.

MITgcm is the first z-coordinate model to simulate circulation in sub-ice-shelf cavities, using its SHELFICE package (Losch 2008), basing heat exchange at the water-ice interface on the boundary layer turbulent exchange coefficient, γ_T (*see* Eq. 7; Jenkins et al. 2001). The ICEFRONT package (Xu et al. 2012) developed later follows a similar thermodynamic approach, allowing simulation of vertical ice walls in the domain. We considered two cases with the MITgcm. The first, the idealized simulation (a simplified wedge shaped lake), is 3 km wide in the East–West (E-W) direction, and 6 km long in the north-south, with depth ranging linearly from 160 m at the north to 10 m at the south and constant depth in E-W direction aside from vertical walls at the extremities. The entire 160-m deep northern boundary is set as a glacial ice face. The second case considered is based on actual bathymetry data for Lake Untersee presented by Wand et al. (2006) (Fig. 1), which is smoothed and adjusted to a maximum depth of 160 m (as found by Wand et al. 1996) and run at lower (Untersee–lowres) and higher (Untersee–hires) resolutions. The subaqueous glacial face is assumed essentially vertical (for both the main Anuchin glacier, and the smaller glacier in the lake's south), and follows the depth contours it intersects. Both cases are located at

71°20′S, giving Coriolis frequency -1.38×10^{-4} rad s^{-1}. We define a cyclic time parameter t for modeling, varying from 0 to 1 through the year, with 0 corresponding to the beginning of summer (September 23rd), 0.5 the end of summer (March 20th), and $1 \approx 0$ the end of winter/beginning of next summer.

Water temperature is initially set to a uniform 1°C throughout in the idealized simulation, and over a number of model runs uniformly to values between 0.4°C and 1.0°C in the Untersee–lowres case, to demonstrate the independence of final state on initial temperature distribution. Water velocity and salinity are initially set to zero everywhere in all simulations. Grid spacing for both lakes (the idealized simulation and Untersee–lowres) is set to $\Delta x=\Delta y=124$ m, with Δz transitioning smoothly from $\Delta z=2$ m at the surface to $\Delta z=15$ m throughout the bulk of the water, to allow long-term equilibrium states to be reached. Once achieved in the Untersee–lowres model, resulting temperature distributions are used as initial conditions in the Untersee–hires simulation, where $\Delta x=\Delta y=62$ m and $\Delta z=1$ m at the surface to $\Delta z=10$ m in the bulk water. The Untersee–hires simulation is not pursued initially as it is much less computationally efficient. The grid sizes for Untersee–lowres model and the idealized simulation are $x\times y\times z=40\times48\times14$ and $48\times24\times14$, respectively, while the Untersee–hires model has $78\times96\times20$ cells. Momentum boundary conditions are free slip at the lakes lateral boundaries, and no-slip (with quadratic bottom friction) at the bottom, as commonly used in lake simulations (Dorostkar et al. 2010). The MDJWF polynomial equation of state (McDougall et al. 2003) is used and we use the 3rd order direct space time (DST) Flux limiter advection scheme for temperature. Time step in integration is $\Delta t \sim 100$ s.

Horizontal Smagorinsky viscosity is chosen as 1.0, as generally appropriate for lake problems (Krámer and Józsa 2005) and found to produce realistic results when compared to field data (Dorostkar et al. 2010), the horizontal biharmonic viscosity is set to 2400 or 300 m^4 s^{-1} in the simulations with horizontal grid spacings of 124 m (lowres) and 62 m (hires), respectively, and implicit vertical viscosity is used together with a background vertical eddy viscosity of 10^{-3} m^2 s^{-1}. Implicit vertical temperature diffusion is used, and temperature diffusivity is set to $1.4\times10^{-7}m^2$ s^{-1}.

Forcing for both cases takes the form of solar radiation from the lake surface, which achieves a yearly average of 2.6 W m^{-2}, with its daily magnitude set to zero for six months (Winter) and sinusoidally varying for six months from $t=0$ to $t=0.5$ (Summer), achieving a peak of 8.2 W m^{-2} at $t=0.25$ (Andersen et al. unpubl). Solar radiation absorption uses the model of Paulson and Simpson (1977), using an absorption length of 30 m, as measured in Lake Untersee (Andersen et al. 2011), and similar to that in other very clear freshwater lakes (Kraus 1972). It is anticipated that in Untersee such a long absorption length may be measured since all light entering the water column is of short wavelength, hence falling into the large absorption length regime of Paulson and Simpson's model, as long wavelengths have been attenuated by the ice cover. It is assumed that the lake surface is wholly covered in ice, with an equal transmissivity in all locations, so small regions without ice cover observed near the lake edge (Wand et al. 2006) are ignored. Any radiation reaching the lake's bottom without being absorbed is deposited into the layer of water immediately above it.

Surface temperature forcing is taken care of by a 0°C fixed boundary condition at the lake's surface. The primary Anuchin glacier and smaller secondary glacier in Untersee's south are simulated with the ICEFRONT package, using dimensionless heat exchange coefficient $\gamma_T \sim 1.1\times10^{-3}$ calculated as recommended by Jenkins et al. (2010). Velocity used in calculating heat transfer (Eq. 7) is the larger of 3 mm s^{-1} or the combined magnitude of horizontal and vertical velocities parallel to the face. The minimum value of 3 mm s^{-1} is chosen as this is roughly the expected magnitude of velocity to develop over short flow lengths and is necessary due to the large model resolution resulting in cells along the bathymetry boundaries where velocity is artificially supressed.

A passive tracer is used in the Untersee–hires model to estimate timescales for mixing through the main homogenous basin of the lake using the PTRACERS package of MITgcm. The same 3rd order DST Flux limiter advection scheme is used, and a diffusivity of $\sim 10^{-9}$ m^2s^{-1} is set, an approximate value for 0_2 and CH_4 near 0°C.

The model's response to transient stimulation, as would result from hypothetical glacial calving, is tested via artificially increasing velocities in groups of cells between 0 and 50 m depth along the main glacier to 1 m s^{-1} perpendicular and away from its face. This involved accelerating more than 1×10^6 m^3 of water in some locations, so while the magnitude of the increased velocity (constrained by requirements for model stability) may be substantially smaller than the maximal values near to a real shock incident, the large volume accelerated meant in terms of energy at least this could correspond (on the scale of Lake Untersee) to a mid to large scale calving event.

Results

Idealized simulation

The simplified bathymetry of the wedge shaped lake (the idealized simulation) provides qualitative estimates for expected circulation in Lake Untersee and may be a generic model for other ice-walled lakes such as Lake Hoare in the Dry Valleys of Antarctica (Simmons et al. 1993; Tyler et al. 1998; Spigel and Priscu 2013) and Phantom Lake on Axel Heiberg Island in the Arctic (Caflisch 1972; Andersen et al. 2002). However, due to fundamental differences in the thermodynamic balance, in particular the magnitude of the lake

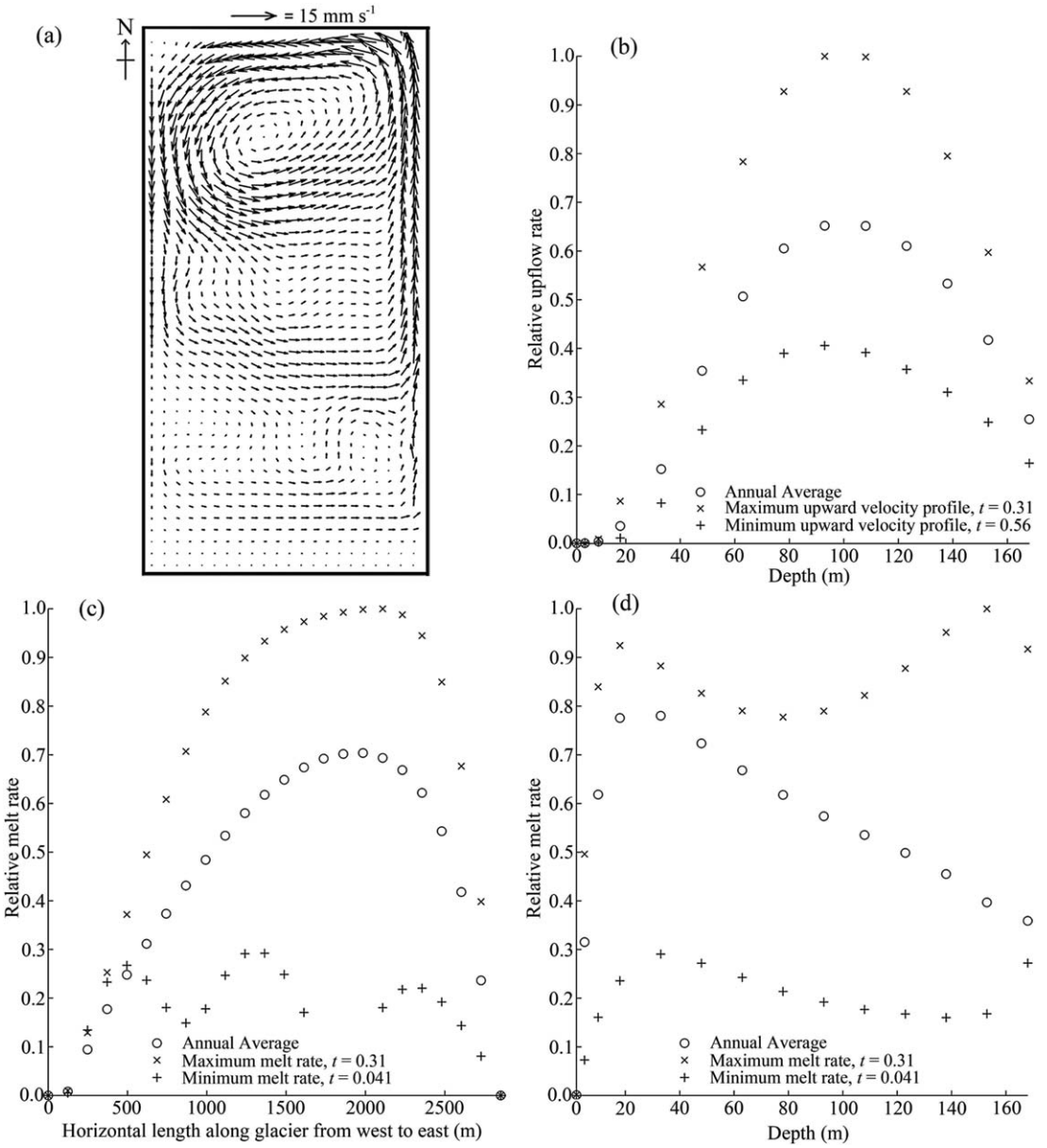

Fig. 3. Idealized Simulation (a) Depth-averaged circulation in the lake at $t = 0.5$. Glacier is along northern face. (b) Dependence of relative (to maximum) upward (z direction) velocity along glacial face on depth (c) Dependence of glacial melt rate on W-E location (moving left to right in a). (d) Dependence of glacial melt rate on depth.

surface area relative to that of the exposed glacial wall, it is likely to give significantly different quantitative results for anticipated velocities and temperatures when compared to the actual Lake Untersee bathymetry.

Circulation in the idealized simulation is found to be anticyclonic at all depths throughout the year, resulting in flow from the east to west along the glacial face. A main gyre (Fig. 3a), as wide as the lake in the E-W direction, extending on average 2.5 km from the glacial face and centred slightly to the west of the lake's centre, persists, and other anticyclonic gyres of similar scale form intermittently over time in more southern areas. The body temperature, T_{body}, defined as the mean temperature in the well mixed (body water) portion of the basin 10 m from the ice cover through to the bottom (which in the case of the idealized simulation, is all water below 10-m depth, and in Untersee, that below 10 m and not within the anoxic basin), varies from a maximum of 1.19°C achieved at the end of summer ($t = 0.5$), to a minimum of 1.11°C at the end of winter ($t = 1$). The standard deviations of T_{body} throughout the lake at those times are 0.013°C and 0.022°C, respectively, demonstrating the temperature's uniformity throughout. Glacial

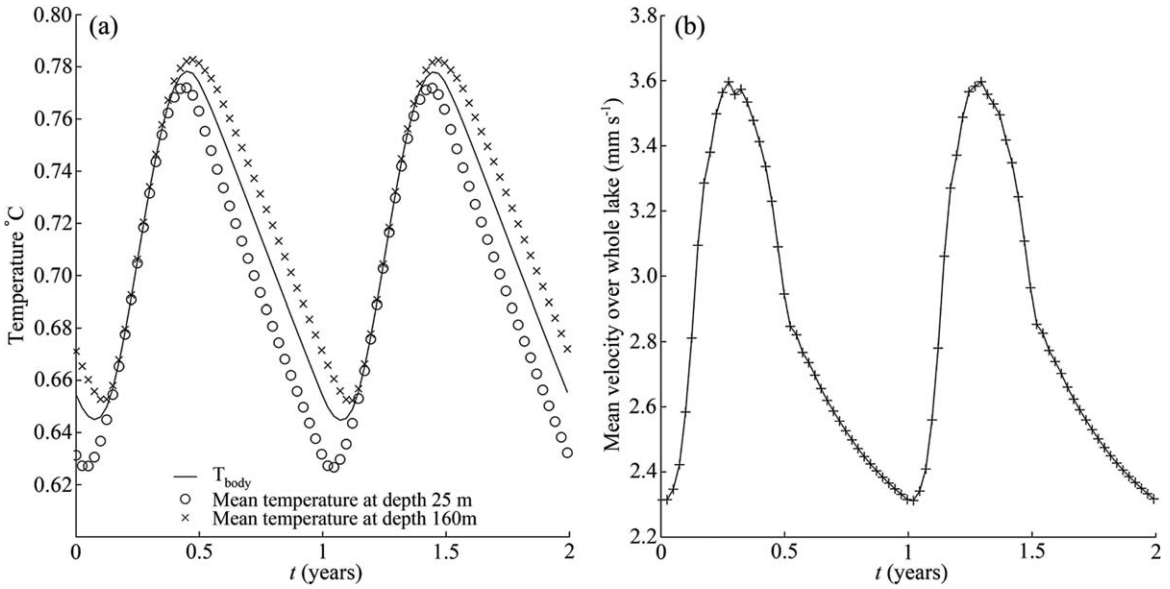

Fig. 4. Annual temperature/velocity trends for 2 yr. (a) Annual temperature trends for the lake body, and water at 25-m and 160-m depth. (b) The mean flow velocity over all areas of Lake Untersee.

melt rates are longitudinally asymmetric (Fig. 3c), peaking to the east of the glacier's center. This is a result of E-W (tangential to glacial face) velocities which reach their greatest at this point, due to the main gyre driving strong northward current toward the glacier along the lake's east side. The melt rate is found on average to peak near 25-m depth (Fig. 3d). The sharp decrease toward zero depth is due to lower temperature water near the surface ice, resulting in a smaller temperature difference between the ice and surrounding water (expressed in Eq. 7), and the decrease in melt rate at depths greater than 25 m is predominantly a result of lower average velocities found at depth in the persistent gyre near the glacial face. Water is found to accelerate up the ice face, with flow taking some time to develop, before reaching a peak velocity near 100-m depth (Fig. 3b). Upward (z) velocities are found to be more than an order of magnitude greater in grid cells adjacent to the ice face than anywhere else in the basin.

Lake Untersee–lowres model

The Lake Untersee–lowres model is run for $\sim$ 30 yr integration time to establish equilibrium conditions in all parts of the basin and to assess their convergence. Circulation takes on the order of weeks to spin-up, similar time scales to those found in other lake models (Huttula et al. 2010). An anticyclonic gyre is formed in front of the glacier face, and basin scale anticyclonic circulation following the outside of the lake is observed (*see* Fig. 4 for the Untersee–hires model). Mean velocities in the well mixed lake body vary with the seasons (Fig. 4b), reaching a peak at $t \sim 0.33$ ($\sim$ January 20th), about two thirds of the way through the summer months, and attaining their minimum at $t \sim 0$, the end of winter ($\sim$ September 22nd).

Body temperature converges to a stable state with annual average $\sim$ 0.71°C in $\sim$ 5-15 yr integration time, achieving the same equilibrium state regardless of initial temperature state. Mean body temperature varies between a minimum of 0.65°C at the start of summer to maximum of 0.78°C at the end (Fig. 4a), giving an annual temperature fluctuation between summer and winter of ΔT_{body}=0.13°C. During summer, temperature is almost constant with depth, however, homogeneity decreases at the end of winter, with a $\Delta T \sim 0.04$°C difference in temperature forming between the basin's bottom and upper water levels. Mean temperature in the anoxic basin, below a depth of $\sim$ 70 m, is found to diverge from the body temperature of the lake, increasing from the initial state at an almost constant rate, until reaching an essentially steady temperature after $\sim$ 25 yr (depending on initial temperature condition) with annual value fluctuating between 3.81°C and 3.84°C. While approaching this state the temperature in the anoxic basin increases at a similar rate to that in the rest of the lake's water during summer, but remains essentially constant during winter. To analytically treat a simplified version of this problem, the heat transfer with the anoxic zone can be assumed as entirely due to solar radiation reaching its top, at $\sim$ 60-m depth. Given an average depth in the region of 80 m, dividing the solar radiation arriving at its top into the height of that water column (20 m) gives a timescale of 22 yr for a 3°C warming of the region, comparable with the timescale found for convergence in modeling.

When run without the small southern glacier (that is, replacing the small southern glacial face with rock) model

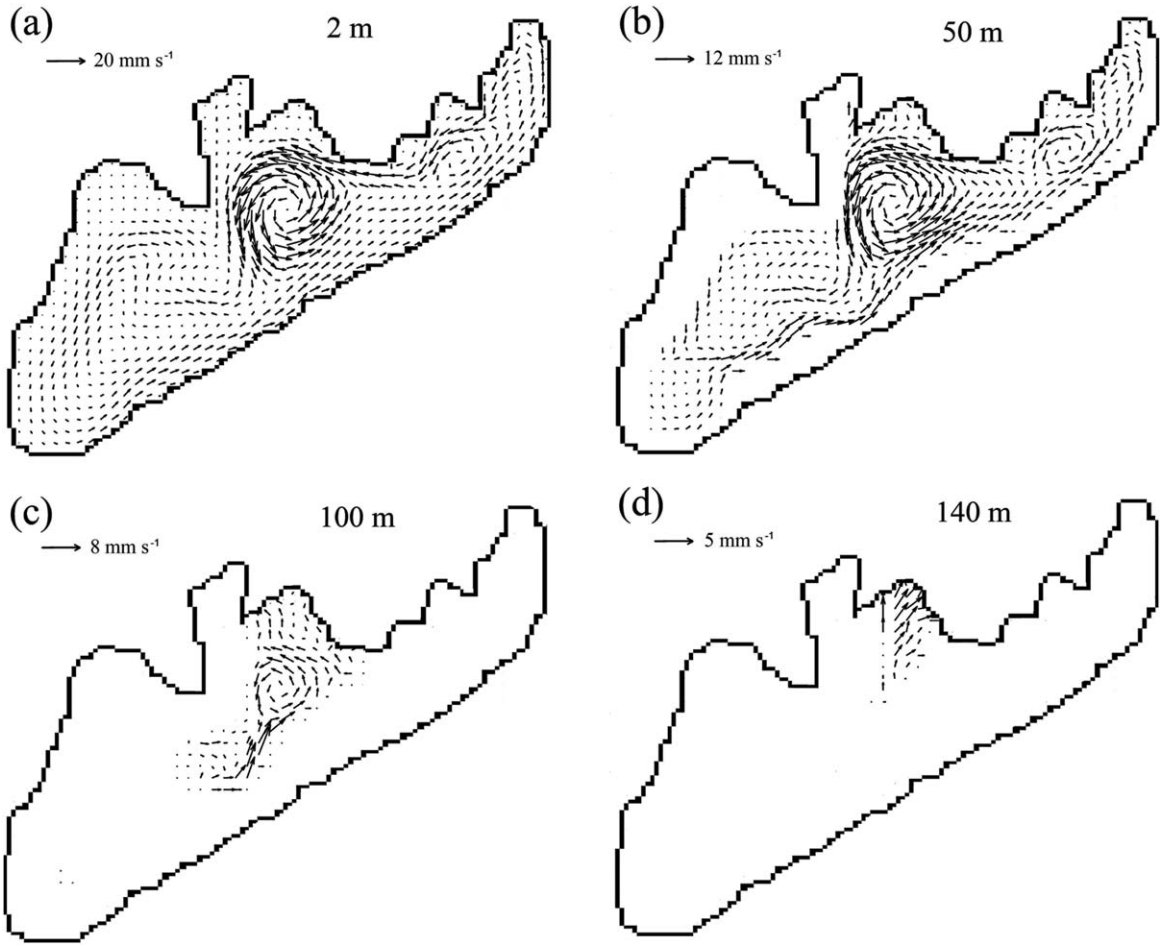

Fig. 5. Horizontal velocity distribution at $t = 0.5$ (mid-March). Circulation diagrams with scale at depths 2, 50, 100, and 140 m for the Lake Untersee–hires model.

results yield qualitatively indistinguishable circulation patterns, a decrease of $\sim$ 1% in lake-wide mean horizontal velocities, and an increase of $\sim 0.01^{\circ}$C in the lake's long-term mean temperature, as would be expected from a slight reduction in the lake's exposed ice are, and hence cooling rate. Removal of both glaciers, resulting in Untersee modeled as a standard perennially ice-covered lake, yields substantially altered long-term behavior. The previous lake-wide gyre is replaced by smaller localized circulation patterns, both cyclonic and anticyclonic, and mean horizontal velocities decrease to 20% of their previous value. Thermodynamic equilibrium, now governed by the balance of incoming solar radiation and heat lost to surface ice cover, attains a long-term mean temperature of $\sim 4.3^{\circ}$C, with no observed temperature discontinuity existing between the lake's main body of water and the Anoxic basin.

Including both glaciers and setting the Coriolis frequency (and hence contribution by Coriolis acceleration to lake dynamics) to zero yields substantially altered circulation; the main anticyclonic gyre disappears in favor of a turnover roughly defined by water above 50-m depth flowing north to south, while that below 50-m depth flows south to north. This results in larger vertical (z direction) velocities at the northern and southern extremities of the lake, which are likely the cause (due to increased velocity and hence heat transfer along the main glacial face) of an observed 0.03°C decrease in mean temperature. Numerically, this change in circulation corresponds to a 30% decrease in mean lake-wide horizontal velocity, while mean vertical velocities increase by 45%.

Lake Untersee–hires model

A higher resolution Untersee model (Untersee–hires) is used to resolve fine aspects of the lake-wide circulation pattern and temperature distributions. This is integrated over 2 yr, with initial temperature distributions approximated from the equilibrium state at $t = 0$ for the Untersee–Lowres model.

Circulation patterns are dominated by an anticyclonic gyre which forms in front of the glacier front, and persists through the water column to $\sim$ 100-m depth (Fig. 5a,b,c). At

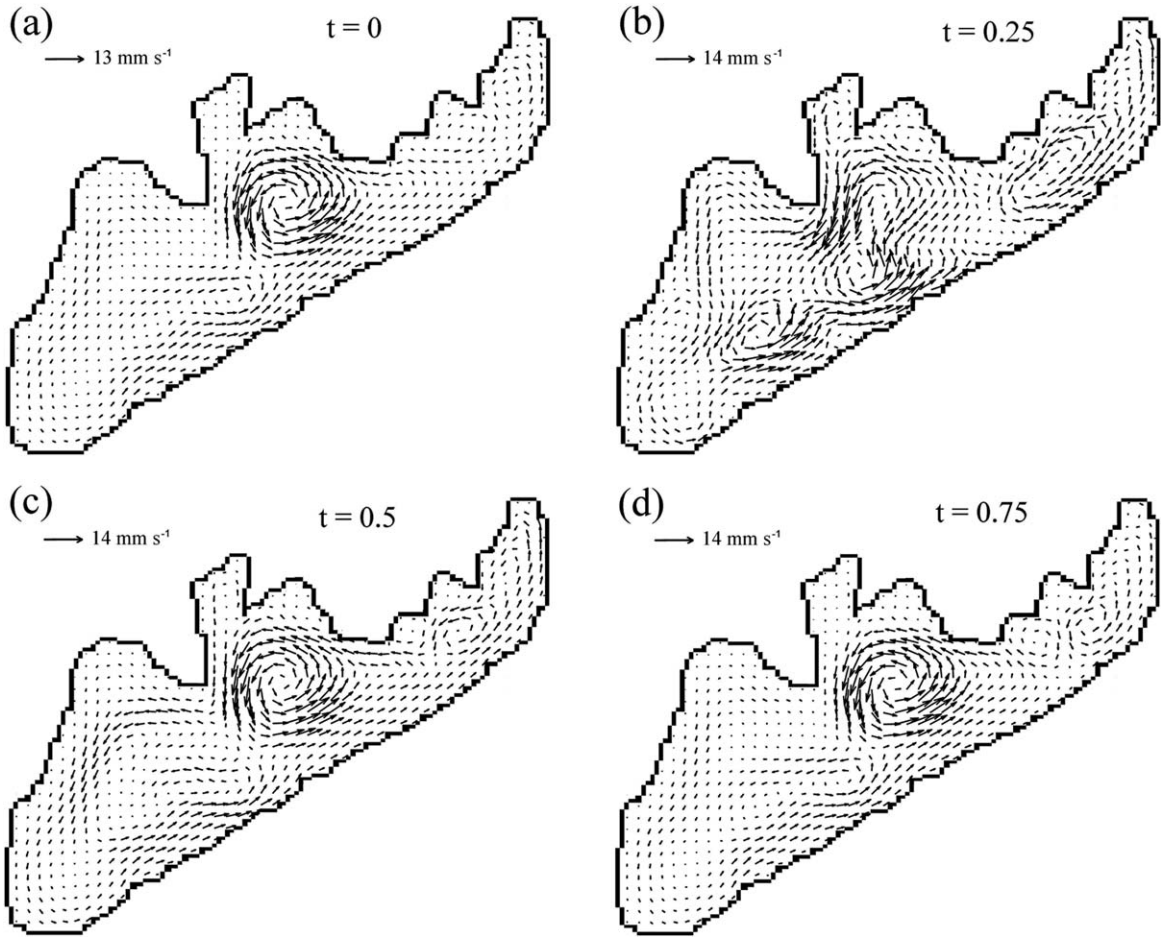

Fig. 6. Depth averaged horizontal velocity distributions over the course of a year, demonstrating a main central gyre in (a - September, c - March, d - June) and the unstable flow patterns during summer (b - December).

greater depths flow is predominantly toward the glacier face (Fig. 5d), with water near the bottom of the lake being drawn toward the glacier before rising up the ice front. There is consistent anticyclonic circulation around the boundary of the lake (clearly demonstrated in Fig. 6c) which has an annual average velocity near the surface of $\sim$ 3 mm s^{-1}. For most of the year, this circulation does not enter the bay in the north-west of the lake (location (c) in Fig. 1), resulting in a lower annual average velocity in this area of $\sim$ 1.2 mm s^{-1}. The anoxic basin displays little thermal mixing, with mean horizontal and vertical velocities of 0.14 mm s^{-1} and 0.002 mm s^{-1}, respectively, below 70-m depth, while the mean horizontal velocity across its top at 50-m depth averages 1.4 mm s^{-1}. Vertical (z direction) velocities in cells adjacent to the glacial face are positive (upward), and attain an annual average of 0.3 mm s^{-1}, but reach maximum values in some areas of $\sim$ 2 mm s^{-1}. By comparison, the annual mean horizontal and vertical velocities throughout the lake are 3.3 mm s^{-1} and 0.08 mm s^{-1}, respectively. Horizontal velocities reach a peak between 10 and 15-m depth, while vertical velocities increase dramatically with depth when close to the ice cover (rising more than three orders of magnitude by 5 m from the surface), but further away change more slowly, increasing by 50% between 40 and 150-m depth. A subsection of the Untersee–hires model, including the main glacier and surrounding $\sim$ 1 km of lake body, was run at halved resolution (32 m in both x and y directions), resulting in a $\sim$ 70% increase in upward velocities along the glacial face.

Circulation patterns through most of the year (Fig. 6) are essentially constant, except for solar radiation peak times near $t = 0.25$ (mid-December). At this point, the central gyre has broken down to some extent (Fig. 6b), and larger velocity flows are found in other areas throughout the lake.

Body temperature in the Untersee–hires model follows the same yearly cycles as in Fig. 4a, reaching uniformity part way through summer, and peaking at $t = 0.5$. The temperature profile (Fig. 7) in the body of the lake is essentially constant below 5-m depth, and varies little at different locations throughout the lake. An abrupt temperature change occurs

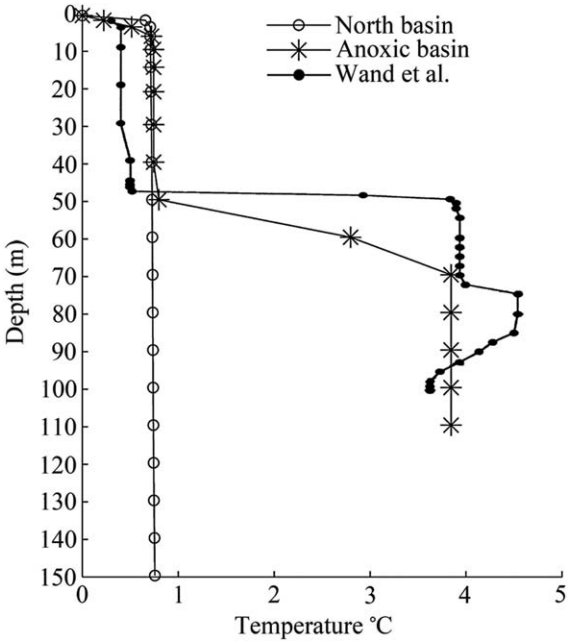

Fig. 7. Temperature profiles for the north basin (200 m from the glacier face) and anoxic basin at $t = 0.25$, mid-December. Data points represent model grid resolution. Field data from Wand et al. (2006) for the anoxic basin included for comparison.

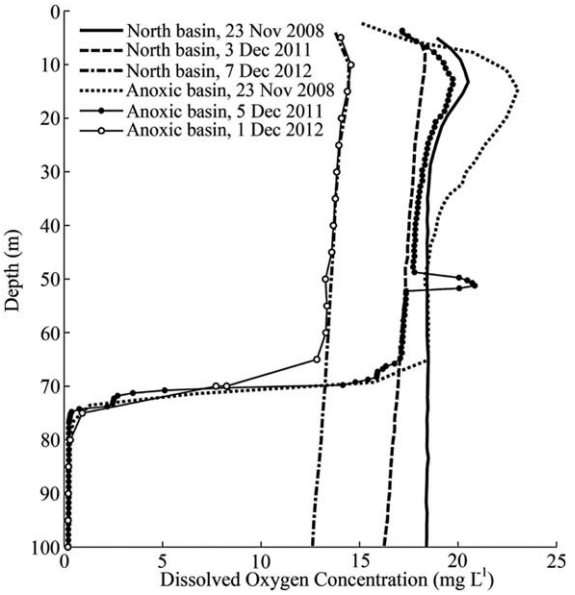

Fig. 9. Dissolved Oxygen profiles measured with regard to depth from the piezometric level of the water column in the north basin (Fig. 1, A) and the anoxic basin (Fig. 1, B) from three expeditions to Lake Untersee.

over $\sim$ 10 m at $\sim$ 55 m depth in the anoxic basin, below which the water maintains a temperature of $\sim 3.8^{\circ}$C throughout the year.

The timescale for distribution of a passive tracer demonstrates roughly one month is required (Fig. 8) between release and its uniform distribution throughout the lake's well mixed body water. After this time, mean tracer concentration in the lake's well mixed body is almost constant with depth, varying by less than 3% between 10 m and 150 m from the surface. Mixing is slower in the top $\sim$ 5 m of water in the north basin, a result of thermal stratification near the surface reducing vertical velocities. In this zone, the mean concentration at one meter depth reaches 60% of the mean in the body water a year after introduction. Mixing is also inhibited in the anoxic basin, where the mean concentration below 70-m depth remains <0.1 % of the lake average a year after introduction. For a tracer introduced into the anoxic basin at 80-m depth, near the top of the anoxic region in our bathymetry (Fig. 7), more than 99% remains within the basin over the course of a year.

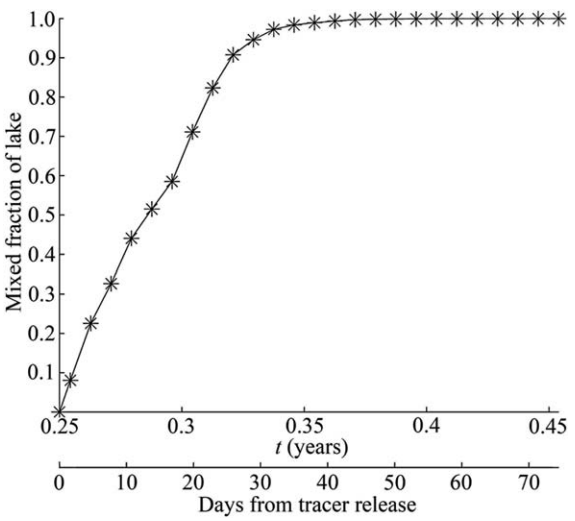

Fig. 8. Tracer mixing in lake, for a tracer released centrally on the glacier at a depth of 80 m at $t = 0.25$. The mixed fraction of the lake is the volume of body water (i.e., below 10 m and not including the anoxic basin) mixed, divided by the total volume to be considered. A cell is defined to be mixed when its tracer concentration is greater than half the mean tracer concentration of all body water cells at that time.

The Anuchin glacier melt rate varies within 30% of its mean value throughout the year, as the temperature (Fig. 4a) and horizontal velocity across it (Fig. 4b) change, resulting in an annual mean melting velocity of 5.6×10^{-8} m s^{-1}, corresponding to a total ice removal rate of 0.039 m^3 s^{-1} across the glacier. Using the estimated cross sectional area of the Anuchin glacier of 0.23 km^2, this melt rate requires the glacier advance at $\sim$ 5.4 m yr^{-1} in order for the ice front to remain stationary in the long term.

Measured oxygen concentration profiles demonstrate good mixing throughout the north basin as anticipated, however substantial humps are observed around 15-m depth in some profiles (Fig. 9), a region in which the model predicted good tracer mixing. Concentration profiles in the Anoxic basin (Fig. 9) demonstrate sharp decreases in oxygen

content near 70-m depth, substantially below the temperature transition depth of 50 m (Fig. 7). While 2008 and 2011 levels are generally similar, 2012 measurements differ considerably in both locations.

To test the sensitivity of the Untersee–hires model on the initial temperature conditions generated from Untersee–lowres model, we scale down the initial body temperature for $t = 0$, changing T_{body} from 0.65°C to 0.33°C. With the lower initial temperature, maximum and mean annual depth averaged velocities are annually 92% and 91%, respectively, of their values when T_{body}=0.65°C, and the annual temperature fluctuation between summer and winter is ΔT_{body}=0.14°C (when adjusted for the rising temperature trend, as the model is not near its equilibrium state). Temperature profiles retain their shape, differing only in terms of T_{body} and circulation patterns are qualitatively the same throughout the year in both cases.

Simulated calving events demonstrate that for shocks generated at various locations along the main glacial wall transient velocity patterns decrease from initial maximums of 1 m s^{-1} to less than 0.1 m s^{-1} in a timeframe of 2-3 h. Shock energy was largely dissipated within 3-4 d; within this time frame mean velocity throughout the lake, initially increased by 30-40% immediately post-shock, fell to within 1% of its anticipated values in a no-shock case, and no significant observable differences in circulation remained. Of note was the fact that some calving events, depending on initial location, produced substantial shock waves in the sheltered bay (Fig. 1, point (c)), although no substantial velocity increases in the anoxic basin region were observed.

Discussion

Temperature distributions and circulation, as well as their annual variations, have been investigated for ice-walled ice-covered lakes. This was done using the MITgcm to simulate two different cases, a simplified wedge shaped lake, followed by cases based on actual bathymetry data from Lake Untersee, Antarctica.

The calculated Rossby radius indicated that flow in the lake would be geostrophic, and this was exhibited in modeling in the form of large anti-cyclonic gyres in both cases considered, which persisted through to near the lake floor (Fig. 5). This was confirmed by model cases in which Coriolis frequency was set to zero, resulting in the disappearance of the main lake-wide gyre in favor of steady north-south flow (with direction changing below 50-m depth), and greater vertical mixing. Circulation patterns are qualitatively steady through winter, but demonstrate substantial differences during summer heating, when solar radiation being deposited in the water column is at a maximum (Fig. 6b). Throughout the year there is circulation around the perimeter of the lake leading to good mixing with most regions, with the major exception being the anoxic basin, which remains effectively shielded from the currents. The velocities in the sheltered bay area (Fig. 1, point (c)), are observed to be consistently less (by about a factor of three) than those in the rest of the lake's north basin, owing predominantly to the peninsula jutting into the lake from the north that shields the region from the lake's central gyre. The lake's perimeter circulation bypasses this area entirely for much of the year, an effect particularly evident in the region's upper water levels (Fig. 5a), and only penetrates strongly into the area during the changing currents near the middle of summer (Fig. 6b).

Upward (z) circulation along the ice face demonstrates good qualitative agreement with expected flow patterns (Fig. 2); fluid is drawn in toward the ice face at the bottom of the system (Fig. 5d), and accelerates upward along the ice, evident in the grid cells adjacent to the ice face demonstrating positive (upward) velocities with substantially larger magnitudes than those elsewhere in the lake. However, the magnitude of vertical velocities along the ice face, averaging 0.3 mm s^{-1} in the Untersee–hires model, compare poorly with the results of Wilson and Lee (1981), which anticipate velocities of $\sim$ 3 mm s^{-1} even over short flow length. This is likely a consequence of horizontal grid coarseness (Δx=62 m for Untersee–hires) in comparison with the boundary layer flows of thickness $\sim 10^{-1}$ m expected for upward motion along the ice face (Wilson and Lee 1981). These boundary layers may grow substantially over the $\sim$ 150-m height of the Anuchin glacier's face, but, remaining more than an order of magnitude smaller than the grid spacing, make underestimation of upward fluid motion magnitude inevitable. The dependence on grid spacing was investigated by Xu et al. (2012) in glacial melting problems, where slow-moving convective plumes were found more reliably resolvable following a decrease in horizontal grid size from 20 m to 2 m, leading to substantial increases in estimated up-flow and hence melt rate, but unchanged patterns of (horizontal) ocean circulation near the glacier face.

Assuming a particle density of $\sim$ 1800 kg m^{-3}, the Stokes particle settling velocity for a sphere is $v \approx 10^6 R^2$, where v is settling velocity (m s^{-1}) and R is the particle radius (m). $v \approx 0.1$ or 2.5 mm s^{-1} for particle radii of 10 or 50 μm, respectively, constraining the maximum size of particles able to rise along the glacial face, with up-flow boundary layer velocities of 2−3 mm s^{-1} anticipated, to $R \sim 50$ μm. For a particle rising to, or originating from, the top of the glacial face, given a 3 mm s^{-1} mean velocity in the lake body, a radius $\leq$ 10 μm is required to travel $\sim$ 2 km, roughly half way down the lake, before reaching the 60-m average depth. To overcome the 50-m deep sill before the anoxic basin $\sim$ 3 km from the glacial face, such a particle would require radius ≤ 7 μm. Mean particle size measured in the sheltered bay area of the lake at $\sim$ 20-m depth is $\sim$ 1 μm (Andersen et al. 2011), a figure in the range predicted by these results, supporting the theory that lake floor sediments may originate in pulses of glacial flour (Chanudet and Filella 2008) that enter

via the glacier and are distributed within the lake (Andersen et al. 2011). However, feldspar crystals of length 50 μm ($R \approx 25\mu$m) are also observed (Andersen et al. 2011), which if travelling $\sim$ 2 km from the glacier to the dive site before reaching 20-m depth (Andersen et al. 2011) would require average flow velocities (assuming density $\sim$ 2560 kg m^{-2}) of $\sim$ 10 cm s^{-1} over their journey, significantly larger than those predicted anywhere in the lake at any time of year, potentially indicating an origin other than the glacial flour—possibly coming from rock transported through the lake ice cover (McKay et al. unpubl).

Tracer transport in the lake body displays mixing time scales on the order of one month, meaning seasonal inputs may result in their concentration fluctuating throughout the well mixed portion of the lake on a subannual time scale. Slower mixing observed in the top few meters is likely due to the thermal stratification near the surface, which resulted in substantially smaller vertical velocities in the region. Measured O_2 profiles in the north basin, and above the anoxic basin, are mostly consistent with this result, demonstrating uniformity throughout the water column, with the exception of an increase in concentration observed near the surface in three of the six readings. This heightened concentration, observed at $\sim$ 15-m depth (the same depth at which modeled horizontal velocity magnitudes are largest) would therefore suggest recent (< 1 month prior) or ongoing introduction of oxygen into the lake. This could be due to summer production of oxygen by photosynthesis or by exsolution of gas as the water freezes to the underside of the ice cover during the winter. A measurement of nitrogen, argon and oxygen and comparison of their ratios would separate these possibilities (Craig et al. 1992; Andersen et al. 1998). The curious layer of increased O_2 at 50-m depth in the profile over the anoxic zone in December 2011 must also represent a recent production and would be mixed on timescales that are much less than a year.

The body temperature, T_{body}, in the lake converged to a long-term average of 0.71°C, varying between 0.65 and 0.78 throughout the year. T_{body} is nearly uniform below $\sim$ 4 m (Fig. 7) as observed in Untersee (Wand et al. 2006), with a slight nonuniformity (Fig. 4) existing during winter. Similar uniformity may be observed in upper layers of seasonally ice covered lakes, where water below the maximum density point is absorbing solar radiation, driving convection (Mironov et al. 2002). Temperature magnitudes differ substantially from temperatures of $\sim$ 0.35°C measured in summer by Wand et al. (2006) and Andersen et al. (2011). Equilibrium T_{body} is dictated by the balance between incoming solar energy (believed to be estimated relatively accurately) and outgoing energy lost to the ice cover (a 0°C boundary condition) and glacial face. Heat lost to melting glacial ice is likely the most poorly constrained factor in this problem due to (a) assumption of a shear glacial wall (no "foot" or surface roughness) following the topological contours of the lake bed, which dictates the area of ice exposed to lake water (and hence total heat loss), (b), large grid sizes resulting in underestimation of velocity along the ice, hence decreased heat transfer (which is proportional to velocity via Eq. 7), despite a minimum velocity of 3 mm s^{-1} being set in heat transfer equations to counter this, and (c), inaccurate estimation of the dimensionless turbulent exchange coefficient.

The sensitivity of melting rate and hence equilibrium temperature on relative glacial face and lake surface areas is demonstrated by the annual average of $T_{\text{body}} \sim$ 1.15°C in the idealized simulation, in which the exposed glacier area is 2.8% of the lake surface area, compared to $T_{\text{body}} \sim$ 0.71°C in the Lake Untersee–lowres model, where the exposed glacial area is 6.2 % of the lake surface area. Calculated melt rates underestimate the glacier velocity at $\sim$ 5.4 m year^{-1}, about two thirds of the measured $\sim$ 9 m year^{-1} (Wand et al. 1999). The theoretical melting velocity of $\sim 8\times10^{-8}$ m s^{-1} (Wilson and Lee 1981) when considering upward boundary layer flow on a small scale, is underestimated by a similar factor (the model predicts an annual average of 5.6×10^{-8} m s^{-1}). This indicates that, in addition to assumptions regarding shape and size of the glacier face, inaccuracies may be due to the approximations inherent in the description of the boundary layer heat transfer that was used in modeling (Jenkins et al. 2001), in particular the dependence on velocities along the ice face that are not being properly resolved in our model (investigated by Xu et al. 2012), as well as the chosen value for turbulent exchange coefficient in Eq. 7.

The anoxic basin converged to a steady temperature $\sim$ 3.8°C, which compares favorably with the measured temperature profile in the area by Wand et al. (2006; Fig. 7), although it does not predict the observed temperature jump to above the maximum density point of water at $\sim$ 75-m depth. Differences to be anticipated due to discretized bathymetry and z grid spacing, making sharp boundaries difficult, and the inaccuracies in idealized simulations, particularly in this case regarding vertical mixing processes. In this regard, the anoxic basin is demonstrating the behavior found in ice-covered (but not ice-walled) lakes: effectively cut off from the effects of the ice wall, the region's water temperature converges to near the maximum density point of freshwater, and low mixing maintains this state over time. While modeled temperature in the anoxic basin diverges from T_{body} slowly due to shielding from lake circulation during winter, it has been suggested that small areas of the surface are not covered by ice in summer, hence receiving increased solar flux, and may be a source of warmer water that flows down and settles into the anoxic basin (Wand et al. 2006), a factor not considered in our model.

Theoretical estimation (via the Blasius Solution for laminar boundary layer thickness) of velocity profiles in the anoxic basin driven by overflow indicate a short velocity transition region, with momentum transfer confined to a $\sim$

3-m boundary layer at the interface between high and low density water. This is exhibited in the Untersee–hires model, where velocity in the anoxic basin is found to be on average more than an order of magnitude slower than that elsewhere in the lake. The Richardson number is very large for the velocities predicted above the anoxic basin in modeling, indicating buoyancy forces so strong that overflow has little effect on mixing at the boundary, which will hence be determined only by molecular diffusion. Long time-scales are found for tracer mixing in the anoxic basin, where over the course of a year neither was a tracer from the body of the lake able to enter nor a tracer from inside the basin able to exit in any substantial amount, despite originating relatively near to the top of the top of the basin. These results demonstrate the anoxic basin's lack of mixing with the main body of water, as observed in field studies of its chemistry (Wand et al. 2006), and support the hypothesis of Wand et al. (2006) that methane emanating from the sediment in the anoxic area is consumed as it diffuses upward and does not reach a depth where it can be mixed into the oxygen rich main body of water.

Mixing with the anoxic region was found not to be altered by simulated mid to large scale calving events, implemented as initial velocity shock conditions, although substantial shock waves were observed to enter the sheltered bay area in the lake's west depending on the initial calving location. Numerical and field studies of mixing due to external forcing events between partially separated regions in other lakes (Umlauf and Lemmin 2005), have demonstrated short-term exchanges of chemistry, as observed here for the sheltered bay area. The fact that Untersee's anoxic region differs in this regard is likely due to the sharp temperature gradient across its entrance, effectively able to repel short-term flow intrusions. Dissipation of energy from shock events took place over 3-4 d on average, leaving no observable changes in circulation patterns following this timeframe.

The Lake Untersee–hires model run from initial temperature conditions more similar to those measured in Lake Untersee (T_{body}=0.33°C) demonstrates at each point during the year little departure from the model in its higher temperature equilibrium state; flow velocity is decreased on average by $\sim$ 10 %, and circulation patterns and temperature profiles remain fundamentally the same. This is done to illustrate that despite underestimates in heat transfer with the glacial wall giving an artificially high T_{body}, many of the model's conclusions regarding mixing, temperature profiles, and velocity magnitude and distribution remain largely unchanged when the temperature of the system is halved to more accurately align with field data. However, adjusting T_{body} does in no way compensate for other results of underestimating glacial wall size and heat transfer (T_{body} is just one of the many parameters they decide), so major adjustments to these may alter results more substantially.

Omitting the small southern glacier resulted in negligible differences in long-term behavior of the lake, demonstrating its domination by the more substantial driving force of the main Anuchin glacier. When both glaciers were removed, creating a more commonly studied perennially ice covered lake, mean velocities decreased to $\sim$ 1 mm s^{-1}, circulation formed a greater number of small-scale gyres, no temperature discontinuity was seen in the anoxic region, and long-term mean temperature increased substantially. These results are broadly in keeping with observations of other ice-covered lakes (Kirillin et al. 2012; Rizk et al. 2014), and demonstrate that the presence of a significantly sized ice-wall in a perennially ice-covered lake presents a new and markedly different regime of temperature distribution and circulatory dynamics.

Grid size had minimal effect on mean horizontal velocities observed throughout the lake, with differences on the order of 5% existing between that of the Untersee–lowres and –hires models throughout the year. However, up-flow velocities along the glacier face in the lowres model were $\sim$ 55% of those in the hires model (in which horizontal grid size is 50% of that in the lowres), and those in the hires model were 60% of that in a submodel of just the main glacial face (where horizontal grid size is 50% of that in the hires), highlighting again the insufficiency of the grid spacing in resolving this aspect of the flow.

Modeling results have demonstrated with some generality that the presence of a substantial subaqueous ice wall in an ice covered lake can, aside from driving down mean lake-wide temperatures, yield large-scale changes in dynamics which may influence the exchange of gases and nutrients in the lake, and thereby affect any life present. These changes include encouragement of larger and more energetic lake-wide mixing systems, along with improved vertical mixing due to up-flow along ice faces, but also allow for decreases in fluid exchange with secluded regions that, even separated by some distance from the ice-wall, develop substantial temperature discontinuities in its presence. Similar effects could be expected to occur in other ice-walled lakes in the Arctic and Antarctic and in fjords with active glaciers. Beyond ice-walled lakes the model results may be relevant to any contained water or reservoir system with an isothermal boundary.

References

Andersen, D. T., McKay, C. P., and Wharton, Jr. R. A. 1998. Dissolved gases in perennially ice-covered lakes of the McMurdo Dry Valleys, Antarctica. Antarct. Sci. **10**: 124–133. doi:10.1017/S0954102098000170

Andersen, D. T., Pollard, W. H., McKay, C. P., and Heldmann, J. 2002. Cold springs in permafrost on Earth and Mars. J. Geophys. Res. **107**: 4-1-4-7. doi:10.1029/2000JE001436

Andersen, D. T., Sumner, D. Y., Hawes, I., Webster-Brown, J., and McKay, C. P. 2011. Discovery of large conical

stromatolites in Lake Untersee, Antarctica. Geobiology **9**: 280–293. doi:10.1111/j.1472-4669.2011.00279.x

ASTM Standard G-173 – 03. 2012. Standard Tables for Reference Solar Spectral Irradiances: Direct Normal and Hemispherical on 37° Tilted Surface.

Belmonte, A., Tilgner, A., and Libchaber, A. 1995. Turbulence and internal waves in side-heated convection. Phys. Rev. E **51**: 5681–5687. doi:10.1103/PhysRevE.51.5681

Blasius, H. 1908. Grenzschichten in Flüssigkeiten mit kleiner Reibung. Z. Math. Phys. **56**: 1–37. Available at: http://naca.central.cranfield.ac.uk/reports/1950/naca-tm-1256.pdf

Caflisch, T. 1972. Limnological investigations on Colour and Phantom Lakes, p. 49-56. In Guidebook to Field Tour Ea2, 22nd Int. Geogr. Congress (Montreal). Axel Heiberg Island Res. Repts., McGill Univ., Misc. Papers.

Carey, V. P., and Gebhat, B. 1981. Visualization of the flow adjacent to a vertical ice surface melting in cold pure water. J. Fluid Mech. **107**: 37–55. doi:10.1017/S0022112081001663

Chanudet, V., and Filella, M. 2008. Size and composition of inorganic colloids in a peri-alpine, glacial flour-rich lake. Geochim. Cosmochim. Acta **72**: 1466–1479. doi:10.1016/j.gca.2008.01.002

Craig, H., Wharton, R. A., and McKay, C. P. 1992. Oxygen supersaturation in ice-covered Antarctic lakes: Biological versus physical contributions. Science **255**: 318–321. doi:10.1126/science.11539819

Dorostkar, A., Boegman, L., Diamessis, P. J., and Pollard, A. 2010. Sensitivity of MITgcm to different model parameters in applicaiton to Cayuga Lake Environmental Hydraulics, p. 373-378. Proceedings of the 6th International Symposium on Environemntal Hydraulics.

Fang, X., and Stefan, H. G. 1996. Dynamics of heat exchange between sediment and water in a lake. Water Resour. Res. **32**: 1719–1727. doi:10.1029/96WR00274

Farmer, D. M., and Carmack, E. 1981. Wind mixing and restratification in a lake near the temperature of maximum density. J. Phys. Oceanogr. **11**: 1516–1533. doi:10.1175/1520-0485(1981)011<1516:WMARIA>2.0.CO;2

Gill, A. E. 1982. Atmosphere-ocean dynamics. Academic Press.

Heimbach, P., and Losch, M. 2012. Adjoint sensitivities of sub-ice-shelf melt rates to oceancirculation under the Pine Island Ice Shelf, West Antarctica. Ann. Glaciol. **53**: 59–69. doi:10.3189/2012/AoG60A025

Hermichen, W. D., Kowski, P., and Wand, U. 1985. Lake Untersee, a first isotope study of the largest freshwater lake in the interior of East Antarctica. Nature **315**: 131–133. doi:10.1038/315131a0

Holland, D. M., and Jenkins, A. 1999. Modelling Thermodynamic ice-ocean interactions at the base of an ice shelf. J. Phys. Oceanogr. **29**: 1787–1800. doi:10.1175/1520-0485(1999)029

Holland, P. R., Jenkins, A., and Holland, D. M. 2008. The response of ice shelf basal melting to variations in ocean temperature. J. Clim. **21**: 2558–2572. doi:10.1175/2007JCLI1909.1

Hondzo, M., and Stefan, H. 1994. Riverbed heat conduction prediction. Water Resour. Res. **30**: 1503–1513. doi:10.1029/93WR03508

Hossain, A., and Rees, D. A. S. 2005. Natural convection flow of water near its density maximum in a rectangular enclosure having isothermal walls with heat generation. Int. J. Heat Mass Transfer **41**: 367–374. doi:10.1007/s00231-004-0551-3

Huttula, T., Pulkkanen, M., Arkhipov, B., Lepparanta, M., Solbakov, V., Shirasawa, K., and Salonen, K. 2010. Modelling circulation in an ice-covered lake. Estonian J. Earth Sci. **59**: 298–309. doi:10.3176/earth.2010.4.06

Jenkins, A., Hellmer, H. H., and Holland, D. M. 2001. The role of meltwater advection in the formulation of conservative boundary conditions at an ice–ocean interface. J Phys. Oceanogr. **31**: 285–296. doi:10.1175/1520-0485(2001)031

Jenkins, A., Nicholls, K. W., and Corr, H. F. J. 2010. Observation and parametrization of ablation at the base of ronne ice shelf, Antarctica. J. Phys. Oceanogr. **40**: 2298–2312. doi:10.1175/2010JPO4317.1

Kirillin, G., Lepparanta, M., Terzhevik, A., Granin, N., Bernhardt, J., Engelhardt, C., Efremova, T., Golosov, S., Palshin, N., Sherstyankin, P., Zdorovennova, G., and Zdorovennov, R. 2012. Physics of seasonally ice-covered lakes: A review. Aquat. Sci. **74**: 659–682. doi:10.1007/s00027-012-0279-y

Kirkpatrick, M. P., Armfield, S. W., and Williamson, N. 2012. Shear driven purging of negatively buoyant fluid from trapezoidal depressions and cavities. Phys. Fluids **25**: 025106. doi:10.1063/1.3680861

Krámer, T., and Józsa, J. 2005. An adaptively refined, finite-volume model of wind-induced currents in lake Neusiedl. Period. Polytech. Civil Eng. **49**: 112–136. Available at: http://www.pp.bme.hu/ci/article/view/575

Kratz, T. K., MacIntyre, S., and Webster, K. W. 2005. Causes and consequences of spatial heterogeneity in lakes, p. 329–347. In G. M. Lovett, C. G. Jones, M. G. Turner, and K. C. Weathers [eds.], Ecosystem function in heterogeneous landscapes. Springer Verlag.

Kraus, E. B. 1972 Atmosphere-ocean interaction. Oxford Univ. Press.

Küblbeck, K., Merker, G. P., and Straub, J. 1980. Advanced numerical computation of two-dimensional time-dependent free convection in cavities. Int. J. Heat Mass Transfer **23**: 203–217. doi:10.1016/0017-9310(80)90197-0

Lee, J. J. 1979. Melting of a vertical ice wall by natural convection in pure or saline water. M. Eng. Thesis, Faculty of Engineering and Applied Science, Memorial Univ.

Loopmann, A., Kaup, E., Klokov, V., Simonov, I., and Haendel, D. 1988. The bathymetry of some lakes of the Antarctic Oases Schirmacher and Untersee, p. 6-14. *In* Martin J [ed.], Limnological Studies in Queen Maud Land (East Antarctica). Academy of Sciences of the Estonian SSR, Arctic and Antarctic Research Institute, Tallinn.

Losch, M. 2008. Modeling ice shelf cavities in a z -coordinate ocean general circulation model. J. Geophys. Res. **133**: C08043. doi:10.1029/2007JC004368

MacIntyre, S., and Melack, J. M. 1995. Vertical and horizontal trans- port in lakes: Linking littoral, benthic and pelagic habitats. J. North Am Benthol Soc. **14**: 599–615. doi:10.2307/1467544

Malm, J., Bengtsson, L., Terzhevik, A., Boyarinov, P., Glinsky, A., Palshin, N., and Petrov, M. 1998. Field study on currents in a shallow, ice-covered lake. Limnol. Oceanogr. **43**: 1669–1979. doi:10.4319/lo.1998.43.7.1669

Marshall, J., Adcroft, A., Hill, C., Perelman, L., and Heisey, C. 1997. A finite-volume, incompressible Navier Stokes model for studies of the ocean on parallel computers. J. Geophys. Res. **102**: 5753–5766. doi:10.1029/96JC02775

McDougall, T. J., Jackett, D. R., Wright, D. G., and Feistel, R. 2003 Accurate and computationally efficient algorithms for potential temperature and density of seawater. J Atmos Oceanic Technol **20**: 730–741. doi:10.1175/1520-0426(2003)20<730:AACEAF>2.0.CO;2

McKay, C. P., Clow, G. D., Andersen, D. T., and Wharton, Jr. R. A. 1994. Light transmission and reflection in perennially ice-covered Lake Hoare, Antarctica. J. Geophys. Res. **99**: 20427–20444. doi:10.1029/94JC01414

Millero, F. J. 1978. Freezing point of seawater. Eighth report of the joint panel of oceanographic tables and standards. UNESCO Tech. Pap. Mar. Sci. **28**: 29–31.

Mironov, D., Terzhevik, A., Kirillin, G., Jonas, T., Malm, J., and Farmer, D. 2002. Radiatively driven convection in ice-covered lakes: Observations, scaling and a mixed layer model. J. Geophys. Res. **107**: 7.1–7.16. doi:10.1029/2001JC000892

Patterson, J. C., and Hamblin, P. F. 1988. Thermal simulation of a lake with winter ice cover. Limnol. Oceanogr. **33**: 323–338. doi:10.4319/lo.1988.33.3.0323

Paulson, C. A., and Simpson, J. J. 1977. Irradiance measurements in the Upper Ocean. J. Phys. Oceanogr. **7**: 952–956. doi:10.1175/1520-0485(1977)007<0952:IMITUO>2.0.CO;2

Petrov, M. P., Terzhevik, A. Y., Zdorovennov, R. E., and Zdorovennova, G. E. 2007. Motion of Water in an Ice-Covered Shallow Lake. Water Res. **34**: 113–122. doi: 10.1134/S0097807807020017

Rizk, W., Kirillin, G., and Lepparanta, M. 2014. Basin-scale circulation and heat fluxes in ice-covered lakes. Limnol. Oceanogr. **59**: 445–464. doi:10.4319/lo.2014.59.2.0445

Rowland, J.C., Travis, B. J., and Wilson, C. J. 2011. The role of advective heat transport in talik development beneath lakes and ponds in discontinuous permafrost. Geophys. Res. Lett. **38**: L17504. doi:10.1029/2011GL048497

Simmons, G. M., Vestal, J. R., and Wharton, R. A. 1993. Environmental regulators of microbial activity in continental Antarctic lakes, p. 491–542. In W. J. Green, E. I. Friedmann [eds.], Physical and biochemical process in Antarctic lakes. Wiley-Liss.

Spigel, R. H., and Priscu, J. C. 2013. Physical Limnology of the Mcmurdo Dry Valleys Lakes. In Ecosystem dynamics in a polar desert: The Mcmurdo Dry Valleys, Antarctica. American Geophysical Union.

Tyler, S. W., Cook, P. G., Butt, A. Z., Thomas, J. M., Doran, P. T., and Lyons, W. B. 1998. Evidence for deep circulation in two perennially ice-covered Antarctic lakes. Limnol. Oceanogr. **43**: 625–635. doi:10.4319/lo.1998.43.4.0625

Umlauf, L., and Lemmin, U. 2005. Interbasin exchange and mixing in the hypolimnion of a large lake: The role of long internal waves. Limnol. Oceanogr. **50**: 1601–1611. doi:10.4319/lo.2005.50.5.1601

Wand, U., and Perlt, J. 1999. Glacial boulders 'floating' on the ice cover of Lake Untersee, East Antarctica. Antarct. Sci. **11**: 256–260. doi:10.1017/S0954102099000310

Wand, U., Samarkin, V. A., Nitzsche, H. M., and Hubberten, H. W. 2006. Biogeochemistry of methane in the permanently ice-covered Lake Untersee, central Dronning Maud Land, East Antarctica. Limnol. Oceanogr. **51**: 1180–1194. doi:10.4319/lo.2006.51.2.1180

Wand, U., Schwab, M., Samarkin, W., and Schachtschneider, D. 1996. Sedimentgeologische Arbeiten während der Expedition Schirmacheroase 1994/95 des AWI, Forschungsstelle Potsdam in Arbeiten der AWI-Forschungsstelle Potsdam in Antarktika, 1994/95 Ber Polarforsch **215**: 73–121.

Wang, C. A., and Wang, S. J. 1988. Multiple similarity solutions of buoyancy induced flows for ice melting in cold pure water. Comput. Math. Appl. **15**: 1007–1017. doi: 10.1016/0898-1221(88)90136-8

Warren, S. G., and Brandt, R. E. 2008. Optical constants of ice from the ultraviolet to the microwave: A revised compilation. J. Geophys. Res. **113**: D14220. doi:10.1029/2007JD009744

Wilson, N. W., and Lee, J. J. 1981. Melting of a vertical ice wall by free convection into fresh water. J. Heat Transfer **103**: 13–17. doi:10.1115/1.3244408

Wüest, A., and Carmack, E. 2000. A priori estimates of mixing and circulation in the hard-to-reach water body of Lake Vostok. Ocean Model. **2**: 29–43. doi:10.1016/S1463-5003(00)00007-X

Xu, Y., Rignot, E., Menemenlis, D., and Koppes, M. 2012. Numerical experiments on subaqueous melting of Greenland tidewater glaciers in response to ocean warming and enhanced subglacial discharge. Ann. Glaciol. **53**: 229–234. doi:10.3189/2012AoG60A139

Yoon, J. B., Lee, J., and Kandaswamy, P. 2009. Transient thermo-solutal convection of water near 4°C with opposing

gradients in a square cavity. Int. J. Heat Mass Transfer **52**: 4835–4850. doi:10.1016/j.ijheatmasstransfer.2009.05.019

Acknowledgments

Primary support for this research was provided by the Tawani Foundation of Chicago; the Trottier Family Foundation, NASA's Exobiology and Astrobiology Programs and the Arctic and Antarctic Research Institute/ Russian Antarctic Expedition. Logistics support was provided by Antarctic Logistics Centre International (ALCI), Cape Town, SA and the Von Braun Center for Science Innovation. We are grateful to Colonel (IL) JN Pritzker IL ARNG (Retired) of the Tawani Foundation, Lorne Trottier of the Trottier Family Foundation, Valery Lukin of the Arctic and Antarctic Research Institute, Marty Kress of VCSI, and fellow team members for their support during the expedition. We also thank the editorial team and two anonymous reviewers for their many insightful comment and suggestions.

Submitted 28 January 2015
Revised 20 February 2015
Accepted 2 March 2015

Associate editor: Craig L. Stevens